Crossovers in the thermal decay of metastable states in discrete systems

Thorsten Dröse and Cristiane Morais-Smith
I. Institut für Theoretische Physik, Universität Hamburg, Jungiusstrasse 9, D-20355 Hamburg, Germany
and
Institut de Physique Théorique, Université de Fribourg, Pérolles, CH-1700 Fribourg, Switzerland
(February 1, 2008)

The thermal decay of linear chains from a metastable state is investigated. A crossover from rigid to elastic decay occurs when the number of particles, the single-particle energy barrier, or the coupling strength between the particles is varied. In the rigid regime, the single-particle energy barrier is small compared to the coupling strength, and the decay occurs via a uniform saddle-point solution, with all degrees of freedom decaying instantly. Increasing the barrier one enters the elastic regime, where the decay is due to bent saddle-point configurations using the elasticity of the chain to lower their activation energy. Close to the rigid-to-elastic crossover, nucleation occurs at the boundaries of the system. However, in large systems, a second crossover from boundary to bulk nucleation can be found within the elastic regime, when the single-particle energy barrier is further increased. We compute the decay rate in the rigid and elastic regimes within the Gaussian approximation. Around the rigid-to-elastic crossover, the calculations are performed beyond the steepest-descent approximation. In this region, the prefactor exhibits a scaling property. The theoretical results are discussed in the context of discrete Josephson transmission lines and pancake vortex stacks that are pinned by columnar defects.
PACS numbers: 64.60.My, 74.50.+r, 74.80.Dm, 74.60.Ge

I. INTRODUCTION

The decay of metastable states in systems with one[1] or more degrees of freedom[2](DOF) has been intensively studied in the last decades[3]. The crossover from rigid to elastic decay[4–6] was studied in systems with one and two DOF by using methods known from the analysis of the crossover from thermal to quantum decay[7–10]. In this work we consider a system with N DOF and investigate crossovers that occur in its thermal decay from a metastable state while tuning an external parameter.

A system localized in a relative minimum of a potential energy surface can escape from the trap due to thermal or quantum fluctuations. At high temperatures the decay process is purely thermal, and most probably occurs through the free-energy lowest-lying saddle point that connects two local minima. In this paper we study a model where the energy surface changes upon varying an external parameter δ. Above a critical value δ_*, the saddle point bifurcates into new lower lying ones, causing an enhancement of the escape rate Γ. In the steepest-descent approximation $\Gamma(\delta)$ and its derivative $\Gamma'(\delta)$ are continuous at δ_*, whereas the second derivative $\Gamma''(\delta_*)$ diverges. This behavior can be interpreted in terms of a second-order phase transition[8] and hence is called crossover of second order.

Experimental measurements concerning the decay of metastable states in dc superdonducting interference devices (SQUID's) were interpreted in terms of a saddle-point splitting of the potential energy[5]. This device consists of a superconducting ring intercepted by two Josephson junctions (JJ's). The phase differences across the junctions play the role of generalized coordinates. The inductance of the circuit couples the two phases. By reducing the bias current I that flows through the system, the decay of the phases changes from a rigid regime[11–13], with the two phases decaying together as if they were rigidly coupled, to an elastic regime, with the phases decaying independently[5].

An interesting question is how such a crossover occurs in more complex systems like in a discrete Josephson transmission line (DJTL), which is a one-dimensional array of N parallelly coupled JJ's. Instead of two DOF, one would then have N coupled DOF. Another example of such a system is a stack of N pancake vortices[14] in a layered superconductor in the presence of columnar defects[15]. A vortex pinned by a columnar defect, but subject to a driving current flowing perpendicular to the magnetic field can escape from the trap by thermal activation. The open question is then whether a transition from a rigid to an elastic behavior can be found in the vortex or the DJTL systems, and also if more crossovers inside the elastic regime would arise due to the different decay possibilities involving the large number of DOF. In this paper we analyze the crossover in the decay process due to a saddle-point bifurcation in systems with $N > 2$ DOF. It turns out that for $N = 3$ the saddle points of the potential energy can still be solved exactly. For larger N we determine them perturbatively. Furthermore, we find that for $N \gg 1$ a second crossover from boundary to bulk nucleation can take place in the elastic regime.

The thermal escape rate $\Gamma_{th} = P \exp(-U_a/k_B T)$ is determined in the rigid and elastic regimes for an arbitrary number of particles, by assuming an overdamped motion out of a weakly metastable state. Far from the saddle-point bifurcation, Γ_{th} is evaluated within the Gaussian approximation, including the pre-exponential factor P. Close to the crossover from rigid decay to boundary nu-

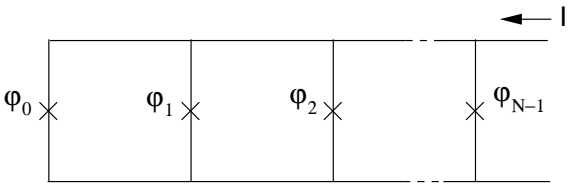

FIG. 1. A current biased one-dimensional array of identical parallelly coupled Josephson junctions, also called a discrete Josephson transmission line. The relevant degrees of freedom are the phase differences φ_n across the junctions.

cleation, we calculate the rate beyond steepest descent and find that P displays a scaling property.

The paper is organized as follows: In Sec. II we introduce the model that can be applied both to DJTL and to pancake vortices in layered superconductors in the presence of a columnar defect. In Sec. III we determine the crossover from rigid decay to elastic boundary nucleation and the corresponding decay diagram. We show that in the elastic regime a second crossover from boundary to bulk nucleation can occur. We evaluate the saddle-point solutions and their activation energies in the three decay regimes. In Sec. IV the thermal escape rate is calculated. Finally, we discuss our results and draw our conclusions in Sec. V.

II. MODEL

A. Free energy

Let us consider a system of N degrees of freedom $\mathbf{u} = (u_0, \ldots, u_{N-1})$, each of them experiencing a single-particle potential $U(u_n)$, and interacting with one another via spring-like nearest-neighbor interactions,

$$\mathcal{E}(\mathbf{u}) = \frac{\kappa}{2} \sum_{n=1}^{N-1} (u_n - u_{n-1})^2 + \sum_{n=0}^{N-1} U(u_n), \qquad (1)$$

where κ is the spring constant. We assume that all the particles are initially situated near a local minimum of the potential U. The coordinates u_n measure the distance of each particle n from this minimum. Close to the local minimum $u_n = 0$, the single-particle potential can be approximated by a cubic parabola,

$$U(u_n) = U_B \left[3\delta \left(\frac{u_n}{R} \right)^2 - 2 \left(\frac{u_n}{R} \right)^3 \right]. \qquad (2)$$

Here $\delta \ll 1$ is a tunable parameter. The constants U_B and R are the characteristic energy and length scales, respectively. At $u_n = R\delta$ the single-particle potential has a maximum. The energy difference between the local minimum and the maximum is $\tilde{U}_B = U(R\delta) = U_B \delta^3$.

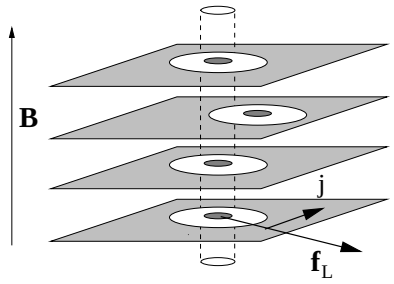

FIG. 2. A stack of "pancakes" produced by a magnetic field $\mathbf{B}$ applied perpendicular to the layers. The pancakes are coupled to each other via magnetic interaction and Josephson currents. A columnar defect pins the vortex. When a current j is flowing through the system, a Lorentz force $\mathbf{f}_L$ acts on the pancakes, reducing the energy barrier the vortex has to overcome to escape from the defect.

Among the physical systems that can be described by Eq. (1) are the DJTL, see Fig. 1. The potential energy of a system of N identical JJ's in the presence of a bias current I is

$$V(\varphi_0, \ldots, \varphi_{N-1}) = \frac{E_J^2}{2LI_c^2} \sum_{n=1}^{N-1} (\varphi_n - \varphi_{n-1})^2 + E_J \sum_{n=0}^{N-1} \left[1 - \cos(\varphi_n) - \frac{I\varphi_n}{NI_c} \right]. \qquad (3)$$

Here the phase differences across the JJ's are given by $\varphi_0, \ldots, \varphi_{N-1}$. The first term in Eq. (3) represents the interaction energy due to the inductances between the loops. Here only the self-inductances of the loops are taken into account, whereas the mutual inductances are neglected[16]. The elastic constant is $\kappa = E_J^2/LI_c^2$, where $E_J = (\Phi_0/2\pi)I_c$ is the Josephson energy, I_c the critical current of a single junction, L is the inductance, and $\Phi_0 = hc/2e$ is the flux quantum. The second term represents the tilted washboard potentials of the driven JJ's that arise due to the relation between currents and gauge invariant phases across the junctions. If we concentrate on the experimentally most interesting limit of currents I close to criticality, $NI_c - I \ll NI_c$, the tilted washboard potential can be well approximated by its cubic expansion, and we can identify $\mathcal{E} = V$ with $u_n = \varphi_n + R\delta/2 - \pi/2$, $U_B = 4\sqrt{2}E_J/3$, $R = 2\sqrt{2}$, and $\delta = \sqrt{(1 - I/NI_c)}$.

Another physical realization of the model described by Eq. (1) is a stack of pancake vortices trapped in a columnar defect, which is artificially introduced in a layered superconductor. Both the magnetic field that produces the pancake vortices and the columnar defect are perpendicular to the superconducting layers; see Fig. 2. Once a bias current $\mathbf{j} = j\mathbf{e}_y$ flows through the layers perpendicular to the magnetic field pointing in the z direction, the pancakes will be driven by the resulting Lorentz force. The corresponding free energy reads

$$\mathcal{F} = \frac{\varepsilon_l}{2s} \sum_{n=1}^{N-1} (\mathbf{u}_n - \mathbf{u}_{n-1})^2 + \sum_{n=0}^{N-1} \left[U_p(\mathbf{u}_n) - \mathbf{f}_L \cdot \mathbf{u}_n) \right]. \tag{4}$$

The displacement of the nth pancake vortex from its equilibrium position in the columnar defect is now given by a two-dimensional vector $\mathbf{u}_n = (u_{n,x}, u_{n,y})$. The first sum in Eq. (4) models the magnetic and Josephson couplings between the layers by elastic interactions between pancakes in adjacent layers[17]. Here $\varepsilon_l = (\varepsilon_0/\gamma^2) \ln(\lambda_{ab}/\xi_{ab})$ is the elastic constant, $\varepsilon_0 = \Phi_0^2/(4\pi\lambda_{ab})^2$ is the vortex self energy, $\gamma = \lambda_c/\lambda_{ab}$ is the anisotropy ratio of the penetration depths λ_c and λ_{ab}, s is the interlayer spacing, and ξ_{ab} is the in-plane coherence length. The second sum contains the columnar defect pinning potentials U_p felt by the single pancakes and the Lorentz force density $\mathbf{f}_L = \Phi_0\ \mathbf{j} \wedge \mathbf{e}_z/c$, where $\mathbf{e}_z$ is the unit vector pointing perpendicular to the planes. The potential U_p is smooth on the length scale ξ_{ab} with a local minimum at the center of the defect. An upper estimate for the depth of the potential well is given by $U_B \approx t\varepsilon_0 \ln(R/\xi_{ab})$, where R is the radius of the columnar defect[15]. The parameter t denotes the superconducting layer thickness. In the large current limit, $\delta = \sqrt{1 - j/j_c} \ll 1$ gives a measure of how close the current j is to the critical current j_c. Then the sum of the pinning and the Lorentz part of the free energy is approximately

$$U_B \sum_{n=0}^{N-1} \left[3\delta \left(\frac{u_{n,x}}{R} \right)^2 - 2 \left(\frac{u_{n,x}}{R} \right)^3 + \frac{3}{2} \left(\frac{u_{n,y}}{R} \right)^2 \right], \tag{5}$$

where we have kept only the terms that are of order δ^3. The terms proportional to $\delta(u_{n,y}/R)^2$ and $u_{n,y}^2 u_{n,x}/R^3$, that are of the order δ^4, have been neglected. Hence the displacements in the y direction are essentially decoupled from the displacements in the x direction. As a consequence, two identical integrals over $u_{n,y}$ appear in the enumerator and in the denominator of the decay rate expression,[2] which will cancel each other. For this reason, we will neglect $u_{n,y}$ in the following. Renaming $u_n = u_{n,x}$, we obtain Eq. (1) with $\kappa = \varepsilon_l/s$.

B. Decay rate

Well above the crossover temperature T_0 that separates the thermally activated decay regime from the quantum tunneling regime, $T \gg T_0$, the escape of the DOF from the pinning potential can be described by a Langevin equation $\eta\ \dot{\mathbf{u}} + \nabla\mathcal{E}(\mathbf{u}) = \mathbf{f}(t)$, assuming that the motion is overdamped. Here η denotes the friction coefficient. If we consider the resistively shunted model for the DJTL, η is the inverse shunting resistance. For the vortex problem, η is given by the Bardeen-Stephen coefficient[18].

The white noise random force $\mathbf{f}(t)$ represents a heat bath at temperature T. It has ensemble averages $\langle f_i(t) \rangle = 0$ and $\langle f_i(t) f_j(t') \rangle = 2\eta k_B T \delta_{ij} \delta(t - t')$. In the limit of weak metastability, where the barrier is much larger than the thermal energy $U_a \gg k_B T$, the corresponding Klein-Kramers equation can be reduced to a Smoluchowsky equation[1]. The escape rate Γ_{th} for the (quasi)stationary case was determined to be[2]

$$\Gamma_{th} = \frac{1}{\eta} \left(\frac{k_B T |\mu_0^s|}{2\pi} \right)^{1/2} \frac{\int_{\mathcal{S}} d^{N-1}\mathbf{u}'\ \mathrm{e}^{-\mathcal{E}(\mathbf{u}')/k_B T}}{\int_{\mathcal{V}} d^N \mathbf{u}\ \mathrm{e}^{-\mathcal{E}(\mathbf{u})/k_B T}}, \tag{6}$$

where $\mathbf{u}' \in \mathcal{S}$, $\mathbf{u} \in \mathcal{V}$, $\mathcal{S}$ is the hypersurface in the configuration space intersecting the saddle point(s) perpendicular to the unstable direction(s), $\mathcal{V}$ is the configuration volume occupied by all metastable solutions and μ_0^s is the curvature of the energy surface $\mathcal{E}(\mathbf{u})$ along the unstable direction evaluated at the saddle point.

Solving Eq. (6) in the steepest-descent approximation, one can derive the Arrhenius law

$$\Gamma_{th} = P(\delta)\ \exp\left(-\frac{U_a(\delta)}{k_B T} \right). \tag{7}$$

The activation energy U_a is obtained by evaluating the energy functional (1) at the saddle-point configuration, which will be done in Sec. III. The computation of the prefactor P is a more involving task. In this case, we have to analyze the spectrum of the curvature matrix $\partial_n \partial_m \mathcal{E}$ at the minimum and at the saddle point, since P describes the contributions to the rate that stem from the fluctuations around the extrema. At a characteristic value $\delta = \delta_*$ the saddle bifurcates indicating a crossover from a rigid regime to an elastic regime. In the crossover region, the steepest-descent approximation cannot be applied. However, even beyond the steepest-descent approximation, the form of Eq. (7) remains valid. The calculations of P will be performed in Sec. IV.

III. SADDLE-POINT SOLUTIONS AND THEIR ACTIVATION ENERGIES

The thermally activated escape from the local minimum $\mathbf{u}_{min} = (0, \ldots, 0)$ of the potential proceeds mainly via the saddle-point solutions $\mathbf{u}_s$ of (1). These unstable stationary solutions satisfy $\nabla_u \mathcal{E}(\mathbf{u}_s) = 0$, and their curvature matrix $\mathbf{H}(\mathbf{u}_s)$ with elements

$$H_{nm}(\mathbf{u}_s) = \frac{\partial^2}{\partial u_n \partial u_m} \mathcal{E}(\mathbf{u}_s) \tag{8}$$

has at least one negative eigenvalue.

A. Saddle-point bifurcation

The saddle point $\mathbf{u}_{rs} = (R\delta, \ldots, R\delta)$, which we call the rigid saddle point (rs), can be readily identified. In Appendix A we calculate the eigenvalues of a curvature

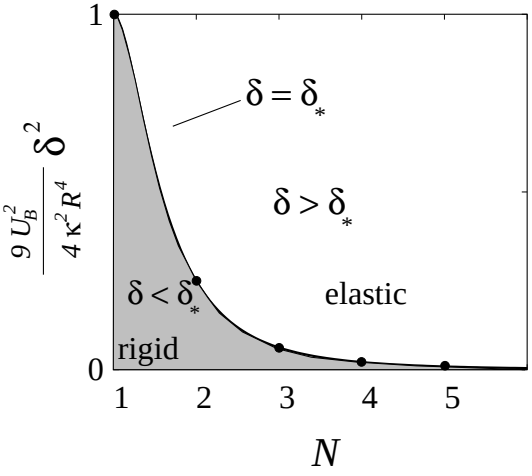

FIG. 3. The decay diagram of a system with a small number of degrees of freedom N. The solid line and the dots indicate the crossover from rigid to elastic decay at $\delta = \delta_*$ as a function of N.

matrix for a uniform extremal solution. Using Eq. (A10) we find the eigenvalues for $H(\mathbf{u}_{rs})$,

$$\mu_n^{rs} = -\frac{6U_B\delta}{R^2} + 4\kappa \sin^2\left(\frac{n\pi}{2N}\right). \tag{9}$$

The lowest eigenvalue $\mu_0^{rs} = -6U_B\delta/R^2 < 0$ indicates that there is at least one unstable direction. It is the only one, if δ is smaller than

$$\delta_* = \frac{2\kappa R^2}{3U_B} \sin^2\left(\frac{\pi}{2N}\right). \tag{10}$$

However, when $\delta \to \delta_*$, the eigenvalue $\mu_1^{rs} = 6U_B(\delta_* - \delta)/R^2$ vanishes. At $\delta = \delta_*$ the saddle splits indicating the existence of an *elastic* saddle-point configuration $\mathbf{u}_{es}$. Below, we will show that for $\delta > \delta_*$ the energy $\mathcal{E}(\mathbf{u}_{es})$ is smaller than $\mathcal{E}(\mathbf{u}_{rs}) = N\tilde{U}_B$. Hence the *elastic* saddle-point configuration $\mathbf{u}_{es}$ instead of the *rigid* one is the most probable configuration that leads to decay. One identifies the energy of the most probable configuration with the activation energy U_a. The saddle-point bifurcation can thus be interpreted as a crossover between two types of decay: the crossover from a *rigid* regime with an activation energy $U_a(\delta \le \delta_*) = N\tilde{U}_B$ to an *elastic* regime with $U_a(\delta > \delta_*) = \mathcal{E}(\mathbf{u}_{es})$. The corresponding decay diagram is shown in Fig. 3.

B. Rigid and elastic saddles

We now calculate the elastic saddle-point solutions. First, we discuss the appearance of the elastic saddle in the crossover regime for arbitrarily many DOF. The evolution of the elastic saddle point with increasing δ is elucidated by analyzing the exactly solvable case of three DOF. Far from the crossover, the three-particle result is used to make an ansatz for the N-particle solutions, which can again be determined perturbatively.

Near the crossover, we expand the elastic solution around the rigid one, $\mathbf{u}_{es} = \mathbf{u}_{rs} + \Delta\mathbf{u}$. Then $\mathcal{E}$ is most conveniently represented in the coordinate system of the principal axis of $H(\mathbf{u}_{rs})$, where $\mathcal{E}$ is diagonal in the coordinates up to second order. The transformation is achieved by rewriting $\Delta\mathbf{u}$ as a trigonometric polynomial,

$$u_n = R\delta\left[1 + \sum_{k=0}^{N-1} q_k \cos\left(\frac{\pi k\,(n+1/2)}{N}\right)\right]. \tag{11}$$

Here the coordinates q_k are the dimensionless amplitudes of the Fourier modes with a wave number k that measure the deviations from the rigid saddle-point solution $u_n^{rs} = R\delta$. In this coordinate system, the energy functional reads

$$\begin{aligned}\mathcal{E}(\mathbf{q}) = N\tilde{U}_B\Bigg[1 - 2q_0^3 + \frac{1}{2}\sum_{k=0}^{N-1}\tilde{\mu}_k^{rs}q_k^2 \\ -3q_0\sum_{k=1}^{N-1}q_k^2 - \frac{1}{2}\sum_{k=1}^{N-1}q_k^2\left(q_{2k} - q_{2(N-k)}\right) \\ -\sum_{m>k=1}^{N-1} q_m q_k\left(q_{m+k} + q_{m-k} - q_{2N-m-k}\right)\Bigg],\end{aligned} \tag{12}$$

where we define $q_k \equiv 0$ for $k < 0$ or $k \ge N$, and $\mathbf{q} = (q_0, \ldots, q_{N-1})$. In the new coordinate system, the dimensionless eigenvalues $\tilde{\mu}_k$ of the curvature matrix are given by $\tilde{\mu}_0 = (R^2/U_B\delta)\mu_0$ and $\tilde{\mu}_k = (R^2/2U_B\delta)\mu_k$ for $k \ne 0$. The different prefactors are due to transformation (11). At the rigid saddle one finds

$$\tilde{\mu}_k^{rs} = \frac{2\kappa R^2}{U_B\delta}\sin^2\left(\frac{\pi k}{2N}\right) - 3 - 3\delta_{0,k}, \tag{13}$$

where $\delta_{0,k}$ is the Kronecker delta function. For $\delta < \delta_*$, where the saddle-point solution is the rigid one with $u_n = R\delta$, all the values $q_n = 0$. The second order expansion of $\mathcal{E}$ around the rigid saddle point reads

$$\mathcal{E}(\mathbf{q}) = N\tilde{U}_B\left(1 + \frac{1}{2}\sum_{k=0}^{N-1}\tilde{\mu}_k^{rs}q_k^2\right). \tag{14}$$

At the crossover, $\tilde{\mu}_1^{rs}$ vanishes and the quadratic approximation of $\mathcal{E}$ becomes independent of q_1. Since large fluctuations in q_1 would not contribute to the free energy, this approximation becomes insufficient within the crossover regime where $\tilde{\mu}_1^{rs} \ll 1$. Thus, in order to describe the free energy contributions of fluctuations in q_1 more properly, higher-order terms in q_1 that arise due to the coupling to the other fluctuation coordinates have to be taken into account. One estimates that $\Delta^2\mathcal{E} \sim q_{n\ne1}q_{m\ne1} \sim q_{n\ne1}q_1^2$. In comparison, the third-order terms $q_kq_mq_n$ with $m, n \ne 1$ are much smaller and

hence can be neglected. Since q_1^2 is only coupled to q_0 and q_2, one finds

$$\mathcal{E}(\mathbf{q}) = N\tilde{U}_B \left[1 + \frac{1}{2}\sum_{k=0}^{N-1} \tilde{\mu}_k^{rs} q_k^2 - 3q_1^2\left(q_0 + \frac{q_2}{2}\right)\right]. \quad (15)$$

In the following, we define the small parameter $\epsilon = (1 - \delta_*/\delta) = -\tilde{\mu}_1^{rs}/3$, which measures the distance from the crossover. It is positive in the elastic regime and negative in the rigid one. Within the crossover regime, $-1 \ll \epsilon \ll 1$. By solving $\nabla\mathcal{E} = 0$, one finds the extrema. In addition to the extrema already found in the rigid regime, an elastic saddle-point solution $\mathbf{q}_{es}$ with a *single* kink emerges slightly below the crossover, for $\delta > \delta_*$,

$$\begin{aligned} q_0^{es} &= \frac{9\epsilon}{2D\tilde{\mu}_0^{rs}}, \\ q_1^{es} &= \left(\frac{3\epsilon}{2D}\right)^{1/2}, \\ q_2^{es} &= \frac{9\epsilon}{4D\tilde{\mu}_2^{rs}}, \\ q_k^{es} &= 0,\ k > 2, \end{aligned} \quad (16)$$

where $\tilde{\mu}_0^{rs}$, $\tilde{\mu}_2^{rs}$, and

$$D = -18/(2\tilde{\mu}_0^{rs}) - 9/(4\tilde{\mu}_2^{rs}) = 3/2 - 9/(4\tilde{\mu}_2^{rs}) \quad (17)$$

are evaluated at the crossover. This *elastic* solution has a lower activation energy $U_a^{es} \approx NU_B\delta^3[1 - C\epsilon^2(\delta)]$ than the stiff solution. Here $C = (54 - 81/\tilde{\mu}_2^{rs})/32D^2$ is a positive constant of the order of unity, since $\tilde{\mu}_2^{rs} \geq 6$ for $N \geq 3$. Since both $U_a(\delta)$ and its derivative $U_a'(\delta)$ are continuous, but $U_a''(\delta)$ is discontinuous at $\delta = \delta_*$, the crossover from rigid to elastic decay is of second order.

In order to illustrate that in our discrete model, close to the crossover, *boundary* nucleation is the dominant process leading to decay in the elastic regime, we will study a chain consisting of three particles, where the saddle-point solutions can be determined exactly. The parameter ϵ can now take any value in the interval $-\infty < \epsilon \ll 1 - \delta_*$. After substituting $\tilde{\mu}_0^{rs} = -6, \tilde{\mu}_1^{rs} = -3\epsilon$ and $\tilde{\mu}_2^{rs} = 6 - 9\epsilon$, the free-energy function reads

$$\begin{aligned} \mathcal{E}(q_0, q_1, q_2) = 3\tilde{U}_B \Big[& 1 - 3q_0^2 - 2q_0^3 \\ & -\frac{3\epsilon}{2}q_1^2 + \left(3 - \frac{9\epsilon}{2}\right)q_2^2 \\ & -3q_0\left(q_1^2 + q_2^2\right) - \frac{q_2}{2}\left(3q_1^2 - q_2^2\right)\Big], \end{aligned} \quad (18)$$

From the extremal condition $\nabla\mathcal{E} = 0$ we calculate the extrema and find that slightly below the crossover in the elastic regime, only $\mathbf{q}_{es} = (q_0^{es}, q_1^{es}, q_2^{es})$, with

$$q_0^{es} = -\frac{2\epsilon}{3}, \quad (19)$$

$$q_1^{es} = (\pm)\left(\frac{4\epsilon}{3} - \epsilon^2\right)^{1/2}, \quad (20)$$

$$q_2^{es} = \frac{\epsilon}{3}, \quad (21)$$

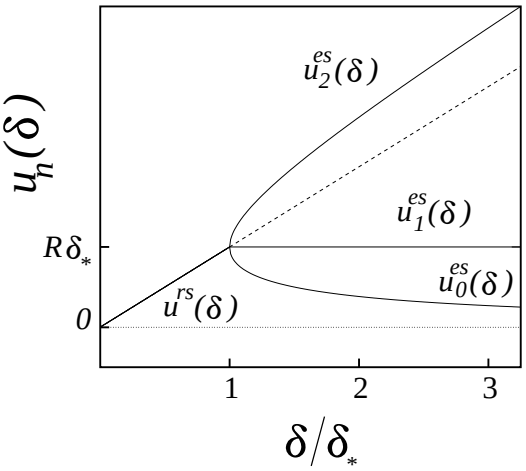

FIG. 4. The saddle-point solutions u_n of a system with three degrees of freedom as a function of the barrier parameter δ/δ_*. For $\delta < \delta_*$ the system escapes rigidly from the local minimum of the potential via a configuration where all the particles are sitting on top of the barrier, $u_n = u^{rs}$. At $\delta = \delta_*$ the saddle splits and the elastic regime is entered for $\delta > \delta_*$. With increasing δ, $u_0 = u_0^{es}$ approaches the minimum, $u_1 = u_1^{es} = R\delta_*$ and the last particle $u_2 = u_2^{es} \to R(\delta + \delta_*)$ is hanging over the maximum of the single-particle potential.

is a possible elastic saddle-point solution. Energetically, the sign in front of q_1^{es} does not have any relevance since q_1 appears only quadratically in $\mathcal{E}$. It arises due to the existence of two degenerate solutions that can mapped into each other by changing the sign of q_1, which is equivalent to a mirror symmetry transformation. Inserting the solutions for the elastic saddle $\mathbf{q}_{es}$ into $\mathcal{E}$, we can represent the free energy as a function of ϵ;

$$\mathcal{E}(\mathbf{q}_{es}) = \tilde{U}_B(3 - 3\epsilon^2 + \epsilon^3). \quad (22)$$

At $\epsilon = 0$ one finds $\mathcal{E}(\mathbf{q}_{es}) = \mathcal{E}(\mathbf{q}_{rs})$. For $\epsilon > 0$, the value of $\mathcal{E}(\mathbf{q}_{es})$ is smaller than that of $\mathcal{E}(\mathbf{q}_{rs})$. Thus there is a smooth crossover from the rigid $\mathbf{q}_{rs}$to the elastic configuration $\mathbf{q}_{es}$, which becomes the most probable one. To summarize, the activation energy of a three particle chain is given by

$$\begin{aligned} U_a^{rs} &= 3U_B\delta^3, \\ U_a^{es} &= U_B\left(\delta^3 + 3\delta_*^2\delta - \delta_*^3\right) \end{aligned} \quad (23)$$

in the rigid and elastic regimes, respectively. In order to visualize the most probable configuration leading to decay, we represent the saddle-point solution in the original coordinates u_0, u_1 and u_2 as a function of the parameter δ. We find that for $\delta > \delta_*$

$$u_0^{es} = \frac{R}{2}\left[\delta + \delta_* - \left(\delta^2 + 2\delta\delta_* - 3\delta_*^2\right)^{1/2}\right], \quad (24)$$

$$u_1^{es} = R\delta_*, \quad (25)$$

$$u_2^{es} = \frac{R}{2}\left[\delta + \delta_* + \left(\delta^2 + 2\delta\delta_* - 3\delta_*^2\right)^{1/2}\right]. \quad (26)$$

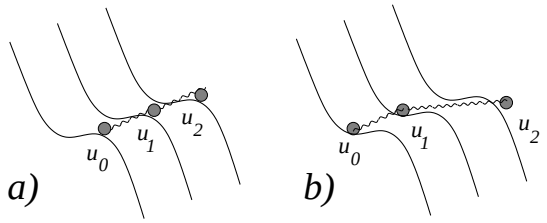

FIG. 5. (a) Rigid saddle-point solutions. (b) Elastic saddle-point solutions.

Note that there exists a second solution with the same energy, which can be found by simply exchanging the indices 0 and 2. The results are displayed in Fig. 4 and illustrated in Fig. 5. By increasing the barrier parameter δ above δ_*, the symmetry along the defect is broken as the elastic saddle-point solution develops. When δ is raised further, particle 0 approaches the potential minimum at $u_{min} = 0$. Particle 1 tries to adjust between its neighbors. It is dragged toward the minimum by particle 0, but, due to the coupling to particle 2, there will be a finite distance between the particles 1 and 0. On the other hand, particle 2 has swapped to the other side of the maximum.

Far in the elastic regime, $\delta/\delta_* \gg N^2$, we can generalize this picture to arbitrary N. Making the ansatz $u_{N-1} \gg u_{N-2} \gg u_{N-3} \sim 0$ we find the approximate solutions of $\nabla\mathcal{E} = 0$,

$$u^{es}_{N-1} \approx R\delta + \kappa R^3/6U_B, \tag{27}$$

$$u^{es}_{N-2} \approx \kappa R^3/6U_B, \tag{28}$$

$$u^{es}_{n\leq N-3} \approx 0, \tag{29}$$

and the equivalent saddle $u_n \to u_{N-1-n}$, with an activation energy

$$U_a = U_B\delta^3\left(1 + \frac{\kappa R^2}{2U_B\delta}\right). \tag{30}$$

The activation energy U_a is displayed in Fig. 6 for $N = 2, 3$, and 4. Note that in this limit the elasticity term $\kappa R^2 \ll 2U_B\delta$ and the activation energy resembles that of a single particle $U_a \sim U_B\delta^3$ with a renormalized barrier parameter. This means that for large δ the system cannot gain much energy by nucleating at the boundary and bulk excitations become important. The bulk saddles are particle like excitations at position m with a double kink,

$$u^{bs}_m \approx R\delta + \kappa R^3/3U_B, \tag{31}$$

$$u^{bs}_{m\pm1} \approx \kappa R^3/6U_B, \tag{32}$$

$$u^{bs}_n \approx 0, \tag{33}$$

where $|m - n| > 1$. They have an activation energy

$$U_a \approx U_B\delta^3\left(1 + \frac{\kappa R^2}{U_B\delta}\right), \tag{34}$$

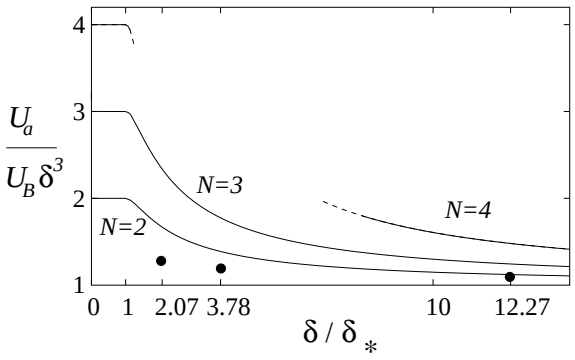

FIG. 6. The activation energy U_a normalized to the activation energy of a single particle $U_B\delta^3$ as a function of the barrier parameter δ for various number of particles N. For $N = 2, 3$ the results are exact, for $N > 3$ the activation energy is calculated perturbatively in the crossover regime $\delta \sim \delta_*$ and in the limit of large δ. The activation energy for $N = 2$ and the experimental data (full dots) are taken from Ref. 5.

which is larger than the activation energy of the elastic boundary saddles. Though energetically not preferable, for $N \gg 1$ the decay can occur via bulk saddle-point solutions if the barrier parameter exceeds a crossover value $\delta > \delta_{bs}$. The crossover to this new regime will be discussed in more detail in Sec. IV.

IV. PREFACTOR

Having determined the activation energies $U_a(\delta)$ for the different regimes, the remaining task is to calculate the prefactor $P(\delta)$ in Eq. (7). Rewritten in terms of $\mathbf{q} = (q_0, \ldots, q_{N-1})$, Eq. (6) reads

$$\Gamma_{th} = \sqrt{\frac{U_B k_B T|\tilde{\mu}^s_0|}{2\pi N\eta^2 R^4\delta}}\,\frac{\int_{-\infty}^{\infty} d^{N-1}\mathbf{q}'\ \mathrm{e}^{-\mathcal{E}(\mathbf{q}')/k_BT}}{\int_{-\infty}^{0} dq_0 \int_{-\infty}^{\infty} d^{N-1}\mathbf{q}''\ \mathrm{e}^{-\mathcal{E}(\mathbf{q})/k_BT}}. \tag{35}$$

Here $\mathbf{q}' = (q^s_0, q_1, \ldots, q_{N-1})$ is running along $\mathcal{S}$ and $\mathbf{q} = (q_0, \mathbf{q}'')$ is probing $\mathcal{V}$. In the denominator, $q_0 < 0$ ensures that the integration is only performed over stable configurations. The additional prefactor arises when transforming the integrals to the q system and taking into account that $\mu^s_0 = U_B\delta\tilde{\mu}^s_0/R^2$.

A. Far from the crossover: Gaussian approximation

In the Gaussian approximation, the integrals in the numerator and in the denominator in Eq. (35) are evaluated by taking into account only the quadratic fluctuations around the saddle point $\mathbf{q}_s$,

$$\mathcal{E}(\mathbf{q}) \approx \mathcal{E}(\mathbf{q}_s) + \frac{N\tilde{U}_B}{2} \sum_{k=0}^{N-1} \tilde{\mu}_k^s (q_k - q_k^s)^2, \tag{36}$$

and the local minimum $\mathbf{q}_{min}$,

$$\mathcal{E}(\mathbf{q}) \approx \mathcal{E}(\mathbf{q}_{min}) + \frac{N\tilde{U}_B}{2} \sum_{k=0}^{N-1} \tilde{\mu}_k^{min} (q_k - q_k^{min})^2, \tag{37}$$

respectively. Thus one obtains a prefactor

$$\begin{aligned} P &= \sum_s \frac{U_B \delta |\tilde{\mu}_0^s|}{2\pi\eta R^2} \left(\prod_{n=0}^{N-1} \frac{\tilde{\mu}_n^{min}}{|\tilde{\mu}_n^s|} \right)^{1/2} \\ &= \sum_s \frac{|\mu_0^s|}{2\pi\eta} \left[\frac{\det H(\mathbf{u}_{min})}{|\det H(\mathbf{u}_s)|} \right]^{1/2}, \end{aligned} \tag{38}$$

where the sum over the saddle index s takes into account the contributions of equivalent saddles. Here $(\tilde{\mu}_n^{min})\mu_n^{min}$ and $(\tilde{\mu}_n^s)\mu_n^s$ are the (dimensionless) eigenvalues of the curvature matrices $H(\mathbf{u}_{min})$ and $H(\mathbf{u}_s)$ evaluated at the local minimum $(\mathbf{q}_{min})\mathbf{u}_{min}$ and the saddles $(\mathbf{q}_s)\mathbf{u}_s$, respectively. In contrast to a system with translational invariance, in the finite systems considered here there is no Goldstone mode of the critical nucleus. Hence, well above and below the crossover, where $\mu_1^s \neq 0$, the evaluation of P is not corrupted by divergences.

In the rigid regime, we take only the energetically lowest-lying saddle into account, and the sum over s reduces to a single contribution. With the determinants $\det H(\mathbf{u}_{min})$ and $\det H(\mathbf{u}_{rs})$ given in Eqs. (A7) and (A9) in Appendix A, we find

$$P(\delta < \delta_*) = \frac{3U_B\delta}{\pi\eta R^2} \left[\frac{\sinh(N\Omega)\tanh(\Omega/2)}{\sin(N\tilde{\Omega})\tan(\tilde{\Omega}/2)} \right]^{1/2}, \tag{39}$$

where $\Omega = 2\ \mathrm{arcsinh}(\omega/2)$ and $\tilde{\Omega} = 2\arcsin(\tilde{\omega}/2)$ with $\omega = \tilde{\omega} = \sqrt{6U_B\delta/\kappa R^2}$. Below the crossover, two equivalent low-energy saddle-point solutions arise, as was discussed in Sec. III. The sum over both saddles gives rise to the factor 2 in

$$P(\delta > \delta_*) = 2\frac{|\mu_0^{es}|}{2\pi\eta} \left[\frac{\det H(\mathbf{u}_{min})}{|\det H(\mathbf{u}_{es})|} \right]^{1/2}. \tag{40}$$

In Eqs. (A11) and (A12) we have estimated the determinant $\det H(\mathbf{u}_{es})$ and the eigenvalue μ_0^{es}, respectively, in the limit $\delta \gg \delta_*$. We obtain

$$P(\delta \gg \delta_*) \approx \frac{6U_B\delta}{\pi\eta R^2} \left[1 + \mathcal{O}(\delta_*/\delta) \right]. \tag{41}$$

As already mentioned in Sec. III, for $N \gg 1$ a crossover to a regime can occur, where the decay dominantly occurs via bulk excitations. The number of DOF N_{bs}, where the crossover from boundary to bulk nucleation occurs, is found by comparing the corresponding rates according to Eq. (7). In the bulk regime, one has approximately N equivalent saddles and thus with Eqs. (A13) and (A14) the prefactor is given by

$$P \approx N\frac{3U_B\delta}{\pi\eta R^2} \left[1 + \mathcal{O}(\delta_*/\delta) \right]. \tag{42}$$

Comparing the rates for boundary and bulk nucleation with U_a given by Eqs. (30) and (34), and P given by Eqs. (41) and (42), respectively, we obtain

$$\delta_{bs} \approx \left[\frac{2k_BT\ln(N/2)}{\kappa R^2} \right]^{1/2}. \tag{43}$$

Note, that within our approximations the choice of the system specific parameters N, R, κ and the temperature T is restricted to values that meet the constraint $\delta_{bs} \ll 1$.

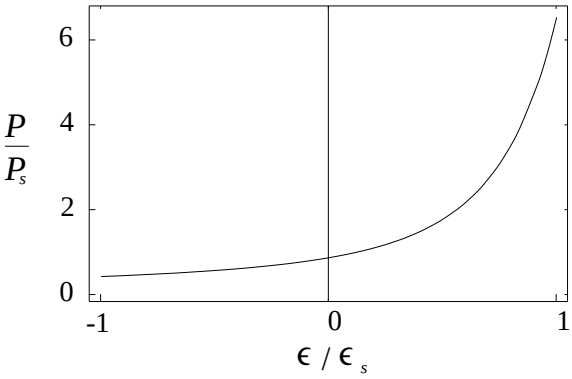

FIG. 7. Scaling property of the prefactor P as a function of δ near δ_*. P/P_s is shown as a function of the distance ϵ from the crossover. Both P_s and ϵ_s are system specific scaling variables.

B. Near the saddle-point bifurcation: Beyond steepest descent

In the crossover regime, where $\delta \to \delta_*$ and hence $|\epsilon| \to 0$, the prefactor calculated in the Gaussian approximation diverges as $P \sim 1/\sqrt{\epsilon}$ due to the vanishing eigenvalue $\tilde{\mu}_1 = -3\epsilon$. The divergence can be regularized by taking into account the third order terms in q_1 in the approximation of $\mathcal{E}(\mathbf{q}')$ around the saddle point in Eq. (35). Defining the system-dependent scaling variables

$$P_s \approx \frac{[54\tanh(\Omega/2)\ \sinh(N\Omega)]^{1/2}\, U_B^{7/4}\delta_*^{9/4}}{\pi^{3/2}\eta R^3 (Nk_BTD)^{1/4}\tan(\pi/2N)}$$

and

$$\epsilon_s = \left(\frac{16k_BTD}{9N\delta_*^3 U_B} \right)^{1/2},$$

we show in Appendix B that

$$P(\epsilon) = P_s F(\epsilon/\epsilon_s), \tag{44}$$

where the function F is found to be

$$F(y) = \begin{cases} \pi\sqrt{\frac{|y|}{2}}\exp(y^2)\left[I_{-1/4}(y^2) - I_{1/4}(y^2)\right], & \delta < \delta_*, \\ 8^{-1/4}\Gamma(1/4), & \delta = \delta_*, \\ \pi\sqrt{\frac{|y|}{2}}\exp(y^2)\left[I_{-\frac{1}{4}}(y^2) + I_{\frac{1}{4}}(y^2)\right], & \delta > \delta_*. \end{cases} \tag{45}$$

For large $|\epsilon/\epsilon_s|$ the prefactor given in Eq. (44) matches with the Gaussian result. However, in the crossover regime, where $|\epsilon/\epsilon_s| < 1$, the Gaussian prefactor deviates strongly from Eq. (44), as expected, since here the Gaussian approximation becomes invalid. Since we considered a metastable situation, where $k_BT \ll U_B\delta^3$, we have $\epsilon_s \ll 1$. Hence, the crossover regime is extremely narrow, $|\delta - \delta_*| \ll \delta_*$. The function $F = P/P_s$, which is shown in Fig. 7, reflects two interesting aspects. First, one realizes that the behavior of the rate is smooth at the crossover. The divergences that occur in the Gaussian approximation are regularized by taking into account higher orders of the fluctuation coordinates. Second, F can be regarded as a scaling function, where the constants ϵ_s and P_s contain the system-specific parameters. The scaling relation is universal in the sense that it does not depend on the details of the considered system. Of course, a constraint is that the crossover must be of second order to guarantee the validity of the perturbative treatment that we applied. However, we have excluded systems with a single-particle potential that enforce a first-order transition from the beginning. Note, that Eq. (44) was found by taking into account only the cubic terms of the modes q_0, q_1, and q_2. These long-wavelength excitations determine the decay process at the crossover, where the discreteness of the system becomes irrelevant. Hence the result can be applied to continuous systems as well. In fact, a similar crossover function is found at the second-order transition from thermal to quantum decay of a single particle in a metastable state[19]. Formally, this theory can also be used to describe a rigid-to-elastic crossover in the thermal decay of an elastic line escaping from a homogeneous defect, but with *periodic* instead of *open* boundary conditions, which we considered here. Note that the scaling function found in Ref. 19 is different from ours. One can indeed show, that the functional form of the scaling function is influenced by the symmetry of the system.

V. DISCUSSIONS AND CONCLUSIONS

We studied the thermal decay of a chain of elastically coupled particles from a metastable state. The metastability arises from each of the particles being trapped in a local minimum of their single-particle potential. The energy barrier that separates the local minimum from energetically lower-lying ones can be tuned by a barrier parameter δ. At $\delta = 0$ the energy barrier vanishes and the metastability ceases to exist. With increasing δ, we find three regimes. For small δ, the decay occurs mainly via a rigid configuration, where all the DOF leave the trap at once. At $\delta_* = 2\kappa R^2 \sin^2(\pi/2N)/3U_B$ a saddle-point bifurcation occurs, which marks a crossover from rigid to elastic motion. For $\delta > \delta_*$ the decay occurs mainly via boundary nucleation. However, at even higher values $1 \gg \delta > \delta_{bs} > \delta_*$ a crossover to bulk nucleation can take place.

Our main goal was to evaluate the thermal decay rate $\Gamma_{th} = P\exp(-U_a/k_BT)$ in the three regimes. This involves the calculation of the prefactor P and the activation energy U_a. The latter is given by the energy $\mathcal{E}$ of the most probable configuration leading to decay, namely, the lowest-lying saddle-point solution. We solved the problem for $N = 3$ particles exactly. Furthermore, we treated the case of an arbitrary number N of DOF perturbatively in the crossover regime and deep in the elastic regime. We have shown how the system uses its elasticity to lower the activation energy in the elastic regime. Whereas in the rigid regime the activation barrier is $U_a^{rs} = NU_B\delta^3$, in the elastic regime near the crossover $U_a^{es} \approx U_a^{rs}(1 - C\epsilon^2)$, where $\epsilon = 1 - \delta_*/\delta$ and $C \sim 1$ is a positive constant that depends on the details of the potential. Increasing δ in the elastic regime, the particles first escape via nucleation at the boundaries with an activation energy $U_a^{es} \sim U_B\delta^3 + \kappa R^2\delta^2/2$, where the first term arises from the potential energy of the activated particle and the second term is the elastic energy of the kink that occurs in the boundary saddle. Due to the imposed free (von Neumann) boundary conditions, this kind of activation is energetically preferred compared to bulk nucleation with an activation energy $U_a^{bs} \sim U_B\delta^3 + \kappa R^2\delta^2$. Since the bulk saddle consists of two kinks, twice the elastic energy is needed to activate a bulk nucleation process. However, in large systems, with $N \gg 1$, bulk nucleation becomes more probable for $1 \gg \delta > \delta_{bs} = \sqrt{2k_BT\ln(N/2)/\kappa R^2}$. Above δ_{bs} the many possibilities to excite a particle somewhere in the bulk, which grow as N in the prefactor P, outnumber the two possibilities of boundary nucleation. At large δ, the elastic interaction between the particles becomes less and less important and the activation energy approaches the energy $U_B\delta^3$ which is needed to excite a single particle over the barrier independently of the others. To discuss the relevant energy scales, we now fix all variables except N. The crossover occurs when the number of DOF is increased above $N_{bs} = 2\exp(\kappa R^2\delta^2/2k_BT)$. Hence, when the elastic coupling is weak and the temperature is high, bulk nucleation already occurs at lower values of N_{bs}. The crossover is thus determined by the ratio of elastic energy and thermal energy.

Second, we determined the prefactor P. Far from the rigid-to-elastic crossover, the calculation of the prefactor P was done in Gaussian approximation both in the rigid

and elastic regimes. Near the crossover, the Gaussian approximation breaks down due to a diverging integral, which is caused by a vanishing eigenvalue of the curvature matrix. By taking into account higher orders in the fluctuation coordinates, we remove the divergence and obtain a smooth behavior of the rate at the crossover. The prefactor of the rate exhibits a scaling property $P/P_s = F(\epsilon/\epsilon_s)$. The function F is universal, but depends on the symmetries of the model. The scaling parameters P_s and ϵ_s are system-specific constants.

At the saddle-point bifurcation $U_a(\delta)$, $U_a'(\delta)$, $P(\delta)$, $P'(\delta)$, and $P''(\delta)$ are continuous, whereas $U_a''(\delta)$ is discontinuous. Hence $\Gamma_{th}(\delta)$ and $\Gamma_{th}'(\delta)$ are continuous, but $\Gamma_{th}''(\delta)$ is discontinuous. Interpreting U_a as a thermodynamic potential, one easily sees the analogy between the crossover described here and a second-order phase transition. This analogy becomes even clearer when the integral in the enumerator in Eq. (6) is interpreted as the reduced partition sum over the DOF transverse to the unstable direction. Note that close to the crossover the discrete structure of the model becomes unimportant, this kind of crossover can also be also found in continuous systems[20–22]. The question arises whether first-order-like transitions could occur also in the thermal decay of elastic chain systems. As in the crossover from thermal to quantum decay[8,23] the type of the crossover depends crucially on the shape of the single-particle potential $U(u_n)$. For a cubic parabola as is discussed in this work, the crossover is of second order. However, one could imagine other physical systems where the single-particle potential has a form that causes a first order transition.

The discrete model that we have used here is quite general. In the following we will discuss the application of the theory to two physical situations, the dynamics of the phases in DJTL's and the thermal creep of pancake vortices in layered superconductors with columnar defects.

DJTL are parallelly coupled one dimensional Josephson-junction arrays, and the N DOF in this case are the phase differences across each of the N Josephson junctions. In current driven DJTL, metastable states occur when the DOF are trapped in a local minimum of the tilted washboard potential common to these systems. For $N = 2$, the problem reduces to the decay of the phases in a current biased dc SQUID[4–6]. Both the rigid decay[13], where the two phases behave as a single one, and the elastic case[5], where the two phases decay one after another, were experimentally observed. In the continuous limit, $N \to \infty$, the system becomes identical to a long JJ. The rigid-to-elastic crossover occurs[21,22] when the junction length L_J becomes of the order of the Josephson length $L_J \sim \pi\lambda_J$. Here we analyzed a model for a DJTL, that provides a system to study the intermediate case of decay from a metastable state with a finite number of DOF. An experimental investigation of the rigid-to-elastic crossover requires that the current I can be driven through the crossover current $I_* = NI_c(1-\delta_*^2)$. An orientation for the choice of the system parameters can be obtained by comparison with the dc-SQUID[5,13], noting that $I_* - NI_c \propto h^2c^2/(e^2L^2I_c^2N^4)$. A systematic experimental study of the rigid-to-elastic crossover as a function of the system parameters L, I_c, and N is still lacking and would be highly desirable. A remaining question was, if additional crossovers occur in systems with a large number of DOF. In addition to the rigid-to-elastic crossover due to a saddle-point bifurcation of the potential energy, we find that in systems with large N a second crossover from boundary to bulk nucleation can take place. DJTL's with a large number of DOF offer the possibility to observe such a crossover by varying system-specific parameters or the temperature.

Let us now discuss our theory in the context of a single stack of pancake vortices trapped in a columnar defect in a layered superconductor. In the presence of a current density j that flows within the layers, the vortices are driven by the resulting Lorentz force. Once thermally activated from the defect, the pancake stack starts to move through the sample until it is trapped by another defect. The resulting motion is called thermal vortex creep. A typical example for a layered system is a high-temperature superconductor (HTSC). A HTSC like YBCO is characterized by an anisotropy $\gamma \sim 5$, and the ratio of the penetration depth to the coherence length is $\lambda_{ab}/\xi_{ab} \sim 100$. The distance between the layers and their thickness are $s \sim t \sim \xi_{ab}$, and the defect radius is $R \sim 2\xi_{ab}$. In order to observe the transition from rigid to elastic decay experimentally, the ratio $(j_c - j_*)/j_c > 0$ must be sufficiently large. However, substituting the defect energy $U_B \sim t\varepsilon_0 \ln(R/\xi_{ab})$ and the elastic energy $\varepsilon_l R^2/s$, with $\varepsilon_l = (\varepsilon_0/\gamma^2)\ln(\lambda_{ab}/\xi_{ab})$, into $(j_c - j_*)/j_c = \delta_*^2$, one finds that even in systems with low anisotropy and a small number of layers $(j_c - j_*)/j_c < 10^{-2}$, indicating that the phenomenon could hardly be observed experimentally in high-T_c superconductors since j_* is very close to j_c. Thus, for large currents $j_c - j \ll j_c$ as considered here, the vortex system turns out to be mainly in the elastic regime where the layered structure of the material is important. Then, the activation barrier U_a is of the order of the single-particle barrier $U_B(1 - j/j_c)^{3/2}$, which can be interpreted as a vortex creep induced by the escape of individual pancakes from the columnar defect[24,25]. This "decoupling" regime can be also entered from the low-current half-loop regime $j \ll j_c$, when the width of the bulk critical nucleus becomes of the order of the layer separation[17]. We find that at low temperatures T the thermal creep is induced by boundary (surface) nucleation. It would be interesting to investigate experimentally if the crossover from bulk to surface nucleation might be observed in thin layered samples. In sum, we calculated analytically the creep rate for coupled particles trapped in a metastable state and found that an interesting behavior arises from the interplay between elasticity, pinning, discreteness and finite-size effects.

ACKNOWLEDGMENTS

We indebted to H. Schmidt, J. Kötzler, G. Blatter, O. S. Wagner, A. V. Ustinov and A. Wallraff for fruitful discussions. Financial support from the DFG-Projekt No. Mo815/1-1 and the Graduiertenkolleg "Physik nanostrukturierter Festkörper," University of Hamburg, is gratefully acknowledged.

APPENDIX A: DETERMINANT AND EIGENVALUES OF THE CURVATURE MATRIX

1. Recurrence relation for the Hessian matrix

As was shown in Sec. IV, the prefactor P of the thermal decay rate is a function of the determinant and the eigenvalues of the curvature matrix evaluated at the relative minimum and the saddle points, respectively, see Eq. (38). The curvature or Hessian matrix $\mathbf{H}_N$ with matrix elements $H_{nm}(\mathbf{u}_0) = \partial_n\partial_m\mathcal{E}(\mathbf{u}_0)$ determines the nature of $\mathcal{E}$ at the extremum $\mathbf{u}_0$. If all eigenvalues of $\mathbf{H}_N(\mathbf{u}_0)$ are negative (positive), $\mathbf{u}_0$ is a relative maximum (minimum). If some of the eigenvalues are positive and some are negative, then $\mathbf{u}_0$ is a saddle point. For $\mathcal{E}(\mathbf{u}_0)$ with $N \geq 3$, the Hessian matrix reads

$$\mathbf{H}_N(\mathbf{u}) = \begin{pmatrix} \partial_0^2\mathcal{E}(\mathbf{u}) & -\kappa & 0 & \cdots & 0 & -\alpha\kappa \\ -\kappa & \ddots & \ddots & & & 0 \\ 0 & \ddots & \ddots & \ddots & & \vdots \\ \vdots & & \ddots & \ddots & \ddots & \vdots \\ 0 & & & \ddots & \ddots & -\kappa \\ -\alpha\kappa & 0 & \cdots & 0 & -\kappa & \partial_{N-1}^2\mathcal{E}(\mathbf{u}) \end{pmatrix}.$$

In the case of open boundary conditions $\alpha = 0$, the diagonal elements are given by

$$\partial_n^2\mathcal{E}(\mathbf{u}) = \begin{cases} \kappa + U''(u_n), & n = 0, N-1 \\ 2\kappa + U''(u_n), & 0 < n < N-1. \end{cases}$$

In the discussion that follows, we introduce

$$D_N = \det_N \begin{pmatrix} 1+x_0 & -1 & 0 & \cdots & 0 \\ -1 & 2+x_1 & -1 & \cdots & \vdots \\ \vdots & \ddots & \ddots & \ddots & \vdots \\ \vdots & \ddots & \ddots & 2+x_{N-2} & -1 \\ 0 & \cdots & 0 & -1 & 1+x_{N-1} \end{pmatrix}, \tag{A1}$$

which is used to calculate both the determinant and the characteristic polynomial of $\mathbf{H}_N$. For example, in order to calculate the determinant of the normalized Hessian $\mathbf{H}_N/\kappa$ for $N > 4$, one sets $x_n = U''(u_n)/\kappa$. Below, we will derive a recurrence relation, which is used to determine D_N in some special cases.

By shifting the last column to the first and then lifting the bottom row to the top, one can rewrite the determinant as

$$D_N = \det_N \begin{pmatrix} 1+x_{N-1} & 0 & 0 & \cdots & 0 & -1 \\ 0 & 1+x_0 & -1 & 0 & \cdots & 0 \\ 0 & -1 & & & & \\ \vdots & 0 & & & & \\ 0 & \vdots & & A_{N-2} & & \\ -1 & 0 & & & & \end{pmatrix},$$

where the $(N-2)\times(N-2)$ matrix A_{N-2} is given by

$$A_{N-2} = \begin{pmatrix} 2+x_1 & -1 & 0 & \cdots & 0 \\ -1 & 2+x_2 & -1 & \ldots & \vdots \\ 0 & \ddots & \ddots & \ddots & 0 \\ \vdots & \ddots & -1 & 2+x_{N-3} & -1 \\ 0 & \cdots & 0 & -1 & 2+x_{N-2} \end{pmatrix}.$$

In the following, we will consider the case where $x_1 = \ldots = x_{N-2} = x$. Note that x_0 and x_{N-1} can be arbitrary.

Expanding D_N, we find with $G_n = \det A_n$

$$\begin{aligned} D_N = (1+x_{N-1})\left[(1+x_0)G_{N-2} - G_{N-3}\right] \\ -(1+x_0)G_{N-3} + G_{N-4}. \end{aligned} \tag{A2}$$

Expanding the determinant G_n according to the last row of A_n, one finds the recursive relation[26] $G_n = (2+x_n)G_{n-1} - G_{n-2}$ that can be rewritten as a difference equation

$$(G_n - G_{n-1}) - (G_{n-1} - G_{n-2}) - x_nG_{n-1} = 0. \tag{A3}$$

The initial conditions are given by the determinants G_1 and G_2,

$$\begin{aligned} G_1 &= 2 + x, \\ G_2 &= (2+x)^2 - 1. \end{aligned} \tag{A4}$$

For $2 \leq N \leq 4$, we can use the recurrence relations for G_n, if we define $G_0 = 1$, $G_{-1} = 0$, and $G_{-2} = -1$.

2. Uniform case

The solution of these difference equations is possible for special cases. We now analyze the uniform case where $x = x_0 = \ldots = x_{N-1}$. Then Eq. (A2) simplifies to

$$D_N = (1+x)^2G_{N-2} - 2(1+x)G_{N-3} + G_{N-4}. \tag{A5}$$

a. Determinant at the relative minimum, $x \geq 0$

We first discuss the case of the local minimum $\mathbf{u} = \mathbf{u}_{min}$, where $x = \omega^2 > 0$. Imposing the initial conditions given by Eq. (A4), one obtains a solution[26] of Eq. (A3),

$$G_{N-1}^{min} = \frac{\sinh(N\Omega)}{\sinh\Omega}, \tag{A6}$$

where

$$\sinh\frac{\Omega}{2} = \frac{\omega}{2}.$$

Using Eqs. (A5) and (A6), we obtain

$$D_N^{min} = \omega^2 G_{N-1}^{min} = 2\tanh\left(\frac{\Omega}{2}\right)\ \sinh(N\Omega). \tag{A7}$$

b. Determinant at the rigid saddle, $x < 0$

In the same way as for the local minimum, one obtains D_N at the rigid saddle $\mathbf{u} = \mathbf{u}_{rs}$ but now with negative $x = -\tilde{\omega}^2 < 0$. One finds

$$G_{N-1}^{rs} = \frac{\sin(N\tilde{\Omega})}{\sin\tilde{\Omega}},$$

where

$$\sin\frac{\tilde{\Omega}}{2} = \frac{\tilde{\omega}}{2}, \tag{A8}$$

and hence

$$D_N^{rs} = 2\tan\left(\frac{\tilde{\Omega}}{2}\right)\ \sin(N\tilde{\Omega}) \tag{A9}$$

c. Eigenvalues

The eigenvalues of $\mathbf{H}_N$ are found by evaluating the roots of the characteristic polynomial, $\det(\mathbf{H}_N - \mu\mathbf{I}) = 0$. We have again a determinant of the form of Eq. (A1), but now with $x_n = U''(u_n)/\kappa - \mu/\kappa$, such that we can define $D_N(\mu) = \kappa^{-N}\det(\mathbf{H}_N - \mu\mathbf{I})$. Using Eq. (A9) we find that the roots where $D_N(\mu) = 0$ are given by $\tilde{\Omega}_m = m\pi/N$, where $m = 0, \ldots, N-1$. Inserting $\tilde{\Omega}_m$ into Eq. (A8) yields $\tilde{\omega}_m = 2\sin(\tilde{\Omega}_m/2)$, hence $D_N(\mu_m) = 0$ for

$$\mu_m = 4\kappa\sin^2\left(\frac{m\pi}{2N}\right) + U''(u_0), \tag{A10}$$

which are the eigenvalues of $\mathbf{H}_N(\mathbf{u}_0)$ for a given uniform extremal solution $\mathbf{u}_0 = (u_0, \ldots, u_0)$.

3. Nonuniform case

Approximate solutions for the determinant and the eigenvalues can be obtained deep in the elastic regime, $\delta/\delta_* \gg 1$.

a. Elastic boundary saddle ($\delta_{bs} > \delta \gg \delta_*$)

For the elastic boundary saddle-point configurations obtained in Eqs. (27)-(29), to highest order in δ/δ_* one finds that $U''(u_0) = \cdots = U''(u_{N-3}) \approx 6U_B\delta/R^2$, $U''(u_{N-2}) \approx 6U_B\delta/R^2 - 2\kappa$, and $U''(u_{N-1}) \approx -6U_B\delta/R^2 - 2\kappa$.

With $x_n = U''(u_n)/\kappa$ one obtains for the determinant up to $\mathcal{O}\left(\delta^{N-2}\right)$

$$D_N^{es} \approx (1 + x_{N-1})(2 + x_{N-2})(1 + x_0)G_{N-3}^{min}. \tag{A11}$$

The ratio D_N^{min}/D_N^{es}, which is needed to calculate the prefactor in the elastic regime is found to be

$$\frac{D_N^{min}}{D_N^{es}} = -1 - \frac{\kappa R^2}{3U_B\delta} + \mathcal{O}\left[(\delta_*/\delta)^2\right].$$

To calculate the eigenvalues, we set again $x_n = U''(u_n)/\kappa - \mu/\kappa$. The characteristic polynomial $D_N(\mu)$ is now up to $\mathcal{O}(\delta^{N-2})$, given by

$$D_N(\mu) \approx (1 + x_{N-1})(2 + x_{N-2})(1 + x_0)G_{N-3}(\mu).$$

Thus, to lowest order in δ, we find that the smallest eigenvalue is

$$\mu_0^{es} \approx = -\kappa - \frac{6U_B\delta}{R^2}. \tag{A12}$$

b. Elastic bulk saddle ($\delta > \delta_{bs}$)

For the elastic bulk saddle-point configurations obtained in Eqs. (31) and (32) to highest order in δ/δ_* one finds for a double kink situated at m, $U''(u_m) \approx -6U_B\delta/R^2 - 4\kappa$, $U''(u_{m\pm1}) \approx 6U_B\delta/R^2 - 4\kappa$, and for $|n - m| > 1$ $U''(u_n) \approx 6U_B\delta/R^2$. With $x_n = U''(u_n)/\kappa$ and using periodic boundary conditions, the determinant is approximately given by

$$D_N^{bs} \approx (2 + x_{m+1})(2 + x_m)(2 + x_{m-1})G_{N-3}^{min}.$$

The ratio D_N^{min}/D_N^{bs} is

$$\frac{D_N^{min}}{D_N^{bs}} = -1 - \frac{4\kappa R^2}{3U_B\delta} + \mathcal{O}\left[(\delta_*/\delta)^2\right]. \tag{A13}$$

The characteristic polynomial $D_N(\mu)$ is now up to $\mathcal{O}(\delta^{N-2})$ given by

$$D_N(\mu) \approx (2+x_{m+1})(2+x_m)(2+x_{m-1})G_{N-3}(\mu),$$

where $x_n = U''(u_n)/\kappa - \mu/\kappa$. Thus, to lowest order in δ, we find that the smallest eigenvalue is

$$\mu_0^{bs} \approx = -2\kappa - \frac{6U_B\delta}{R^2}. \tag{A14}$$

APPENDIX B: PREFACTOR IN THE CROSSOVER REGIME

1. Rigid regime ($\delta \lesssim \delta_*$)

For $\delta \to \delta_*$, both the eigenvalue μ_1^{rs} and the determinant D_N^{rs} vanish. Hence the Gaussian integral containing μ_1^{rs} in Eq. (38) diverges, and third-order terms in q_1 have to be taken into account. In the rigid regime, the third-order expansion of $\mathcal{E}$ in q_1 is given by Eq. (15). The contributions to P of all degrees of freedom except $q_1 \in \mathcal{S}$ are found by Gaussian integration:

$$P = \frac{U_B\delta}{2\pi\eta R^2}\left(\frac{|\tilde{\mu}_0^{rs}|\prod_{n=0}^{N-1}\tilde{\mu}_n^{min}}{\prod_{n=2}^{N-1}\tilde{\mu}_n^{rs}}\right)^{1/2}\left(\frac{NU_B\delta^3}{2\pi k_BT}\right)^{1/2} \times \int_{-\infty}^{\infty} dq_1 \exp\left[-\frac{N\tilde{U}_B}{2k_BT}\left(\tilde{\mu}_1^{rs}q_1^2 + Dq_1^4\right)\right]. \tag{B1}$$

In the following we first derive an approximate expression for $\prod \tilde{\mu}_n^{min}/\prod_{n\neq 1}\tilde{\mu}_n^{rs}$ and then evaluate the remaining integral over q_1.

For the calculation of the product term we use the relation $\prod \tilde{\mu}_n^{min}/\prod_{n\neq 1}\tilde{\mu}_n^{rs} = \tilde{\mu}_1^{rs}D_N^{min}/D_N^{rs}$. Let us analyze D_N^{rs} for $\tilde{\mu}_1^{rs}$ close to zero. Recall that

$$\tilde{\omega}^2 = -\frac{U''(u_0)}{\kappa} = 4\sin^2\left(\frac{\pi}{2N}\right) - \frac{\mu_1^{rs}}{\kappa}.$$

Inserting this expression into Eq. (A8) in the limit of small μ_1^{rs}, we find

$$\tilde{\Omega} \approx \frac{\pi}{N} - \frac{\mu_1^{rs}}{2\kappa\sin(\pi/N)},$$

such that, to lowest order in μ_1^{rs},

$$\sin(N\tilde{\Omega}) \approx \frac{N\mu_1^{rs}}{2\kappa\sin(\pi/N)},$$

and

$$\tan\left(\frac{\tilde{\Omega}}{2}\right) \approx \tan\left(\frac{\pi}{2N}\right).$$

Hence

$$\tilde{\mu}_1^{rs}\frac{D_N^{min}}{D_N^{rs}} = -\frac{4\kappa}{N}\cos^2\left(\frac{\pi}{2N}\right)\tanh\left(\frac{\Omega}{2}\right)\sinh(N\Omega).$$

The integration over q_1 yields

$$\int_{-\infty}^{\infty} dq_1 \exp\left[-\frac{N\tilde{U}_B}{2k_BT}\left(\tilde{\mu}_1^{rs}q_1^2 + Dq_1^4\right)\right] = \frac{1}{2}\sqrt{\frac{\tilde{\mu}_1^{rs}}{D}}\exp\left[\frac{N\tilde{U}_B(\tilde{\mu}_1^{rs})^2}{16k_BTD}\right]K_{1/4}\left[\frac{N\tilde{U}_B(\tilde{\mu}_1^{rs})^2}{16k_BTD}\right], \tag{B2}$$

where D as defined above in Eq. (17) arises during the Gaussian integrations over q_0 and q_2. $K_{1/4}$ is the modified Bessel function. We make the substitution $\tilde{\mu}_1^{rs} = -3\epsilon$. After defining

$$P_s = \left(\frac{U_B^2\delta^2|\tilde{\mu}_0^{rs}|\prod_{n=0}^{N-1}\tilde{\mu}_n^{min}}{8\pi^3\eta^2R^4\prod_{n=2}^{N-1}\tilde{\mu}_n^{rs}}\right)^{1/2}\left(\frac{N\delta^3U_B}{k_BTD}\right)^{1/4} \approx \frac{[54\tanh(\Omega/2)\ \sinh(N\Omega)]^{1/2}\,U_B^{7/4}\delta_*^{9/4}}{\pi^{3/2}\eta R^3(Nk_BTD)^{1/4}\tan(\pi/2N)} \tag{B3}$$

and

$$\epsilon_s = \left(\frac{16k_BTD}{9N\delta_*^3U_B}\right)^{1/2}, \tag{B4}$$

which are constants to leading order in ϵ, we obtain the prefactor of the rate for the rigid region of the crossover regime $\delta \lesssim \delta_*$:,

$$P(\epsilon) = \frac{\pi P_s}{\sqrt{2}}\ \sqrt{\left|\frac{\epsilon}{\epsilon_s}\right|}\left[I_{-1/4}\left(\frac{\epsilon^2}{\epsilon_s^2}\right) - I_{1/4}\left(\frac{\epsilon^2}{\epsilon_s^2}\right)\right]\exp\left(\frac{\epsilon^2}{\epsilon_s^2}\right). \tag{B5}$$

2. Elastic regime ($\delta \gtrsim \delta_*$)

In the elastic regime near the crossover, where $\epsilon \gtrsim 0$, we expand $\mathcal{E}(\mathbf{q})$ around the perturbative elastic saddle-point solution (16),

$$\mathcal{E}(\mathbf{q}) = \mathcal{E}(\mathbf{q}_{es}) + \frac{1}{2}\mathcal{E}^{(2)}(\{\xi_k\}) + \frac{1}{6}\mathcal{E}^{(3)}(\{\xi_k\}),$$

where $\mathcal{E}^{(2)}$ and $\mathcal{E}^{(3)}$ contain the terms of second and third order, respectively, and $\xi_k = q_k - q_k^{es}$ are the fluctuations around the elastic saddle point. By introducing the shifted fluctuation coordinates for $m \neq 1$,

$$\hat{\xi}_m = \xi_m + \frac{2q_1^{es}\xi_1 A_m}{\tilde{\mu}_m^{rs}},$$

with $A_0 = -3$, $A_2 = -3/2$ and $A_{i>2} = 0$, we find, for the quadratic part to leading order in ϵ,

$$\mathcal{E}^{(2)} = -2\tilde{\mu}_1^{rs}\xi_1^2 + \sum_{m\neq 1}\tilde{\mu}_m^{rs}\hat{\xi}_m^{\,2}.$$

Note that $\tilde{\mu}_m^{rs}$ are the dimensionless eigenvalues evaluated at the *rigid* saddle-point configuration. Within the

crossover regime, to leading order in ϵ, the eigenvalues at the elastic saddle-point solution $\tilde{\mu}^{es}_{i\neq 1} = \tilde{\mu}^{rs}_{i\neq 1}$ are independent of ϵ, except $\tilde{\mu}^{es}_1 = -2\tilde{\mu}^{rs}_1 = 2\epsilon/3$. The higher order contributions to the expansion read

$$\frac{1}{6}\mathcal{E}^{(3)} = \left(\sum_{m\neq 1} A_m \hat{\xi}_m\right)\xi_1^2 + 2Dq_1^{es}\xi_1^3.$$

Transforming the fluctuation coordinates a second time,

$$\tilde{\xi}_{m\neq 1} = \hat{\xi}_m + \frac{A_m}{\tilde{\mu}^{rs}_m}\xi_1^2,$$
$$\tilde{\xi}_1 = \xi_1 + q_1^{es},$$

we find

$$\mathcal{E}(\mathbf{q}) = \mathcal{E}(\mathbf{q_{es}}) + \frac{1}{2}\sum_{m\neq 1}\tilde{\mu}^{rs}_m \tilde{\xi}_m^{\,2} + \frac{D}{2}\left[\tilde{\xi}_1^{\,2} - (q_1^{es})^2\right]^2.$$

By using $(q_1^{es})^2 = -\mu_1^{rs}/2D = 3\epsilon/2D$, we evaluate the integrals as in the previous paragraph,[27]

$$\int_{-\infty}^{\infty} d\tilde{\xi}_1 \exp\left\{-\frac{D}{2k_BT}\left[\tilde{\xi}_1^{\,2} - (q_1^{es})^2\right]^2\right\}$$
$$= \frac{\pi}{2\sqrt{2}}\sqrt{\left|\frac{\tilde{\mu}_1^{rs}}{D}\right|}\left\{I_{-1/4}\left[\frac{(\tilde{\mu}_1^{rs})^2}{16k_BTD}\right] + I_{1/4}\left[\frac{(\tilde{\mu}_1^{rs})^2}{16k_BTD}\right]\right\} \quad \text{(B6)}$$
$$\times\ \exp\left[-\frac{(\tilde{\mu}_1^{rs})^2}{16k_BTD}\right],$$

where $I_{1/4}$ and $I_{-1/4}$ are modified Bessel functions. The prefactor of the rate for the elastic regime $\delta \gtrsim \delta_*$ in the crossover region then reads

$$P(\epsilon) = \frac{\pi P_s}{\sqrt{2}}\ \sqrt{\frac{\epsilon}{\epsilon_s}}\left[I_{-1/4}\left(\frac{\epsilon^2}{\epsilon_s^2}\right) + I_{1/4}\left(\frac{\epsilon^2}{\epsilon_s^2}\right)\right]\exp\left(\frac{\epsilon^2}{\epsilon_s^2}\right). \quad \text{(B7)}$$

[1] H. A. Kramers, Physica **7**, 284 (1940).
[2] J. S. Langer, Ann. Phys. (N.Y.) **41**, 108 (1967); Phys. Rev. Lett. **21**, 973 (1968); Ann. Phys. (N.Y.) **54**, 258 (1969).
[3] P. Hänggi, P. Talkner, and M. Borkovec, Rev. Mod. Phys. **62**, 251 (1990).
[4] B. Ivlev and Y. N. Ovchinnikov, Zh. Eksp. Theor. Fiz. **93**, 668 (1987) [Sov. Phys. JETP **66**, 378 (1987)].
[5] V. Lefreve-Seguin *et al.* Phys. Rev. B **46**, 5507 (1992).
[6] C. Morais Smith, B. Ivlev, and G. Blatter, Phys. Rev. B **49**, 4033 (1994).
[7] I. K. Affleck, Phys. Rev. Lett. **46**, 388 (1981).
[8] A. I. Larkin and Y. N. Ovchinnikov, Pis'ma Zh. Eksp. Theor. Fiz. **37**, 322 (1983) [JETP Lett. **37**, 382 (1983)].
[9] H. Grabert and U. Weiss, Phys. Rev. Lett. **53**, 1787 (1984).
[10] U. Weiss, in *Quantum Dissipative Systems*, Vol. 2 of *Series in Modern Condensed Matter Physics*, 2nd ed., edited by I. E. Dzyaloshinski, S. O. Lundquist, and Y. Lu (World Scientific, Singapore, 1999).
[11] Y.-C. Chen, J. Low Temp. Phys. **65**, 133 (1986).
[12] F. Sharifi, J. L. Gavilano, and D. J. V. Harlingen, Phys. Rev. Lett. **61**, 742 (1988).
[13] S. Han, J. Lapointe, and J. E. Lukens, Phys. Rev. Lett. **63**, 1712 (1989).
[14] J. R. Clem, Phys. Rev. B **43**, 7837 (1991).
[15] G. Blatter, *et al.* , Rev. Mod. Phys. **66**, 1125 (1994).
[16] R. D. Bock, J. R. Phillips, H. J. S. van der Zant, and T. P. Orlando, Phys. Rev. B **49**, 10009 (1994).
[17] A. E. Koshelev, P. Le Doussal, and V. M. Vinokur, Phys. Rev. B **53**, R8855 (1996).
[18] J. Bardeen and M. J. Stephen , Phys. Rev. **140**, A 1197 (1965).
[19] H. Grabert, P. Olschowski, and U. Weiss, Phys. Rev. B **36**, 1931 (1987).
[20] T. Christen, Phys. Rev. E **51**, 604 (1995); Europhys. Lett. **31**, 181 (1995).
[21] H. Simanjuntak and L. Gunther, Phys. Rev. B **42**, 930 (1990).
[22] M. G. Castellano *et al.*, Phys. Rev. B **54**, 15417 (1996).
[23] E. M. Chudnovsky, Phys. Rev. A **46**, 8011 (1992).
[24] E. H. Brandt, Europhys. Lett. **18**, 635 (1992).
[25] D. R. Nelson and V. M. Vinokur, Phys. Rev. Lett. **68**, 2398 (1992).
[26] I. M. Gelfand and A. M. Yaglom, J. Math. Phys. **48**, 1 (1960).
[27] I. S. Gradshteyn and I. M. Ryzhik, *Table of Integrals, Series, and Products*, 5th ed., edited by A. Jeffrey (Academic Press, London, 1994).